LBL-38117
UC-1600

ERNEST ORLANDO LAWRENCE
BERKELEY NATIONAL LABORATORY

Surface Temperatures of Insulated Glazing Units: Infrared Thermography Laboratory Measurements

B.T. Griffith, D. Türler, and D. Arasteh
Energy and Environment Division

December 1995
Presented at the
ASHRAE Symposium
San Antonio, TX,
June 22–26, 1996,
and to be published in
the Proceedings

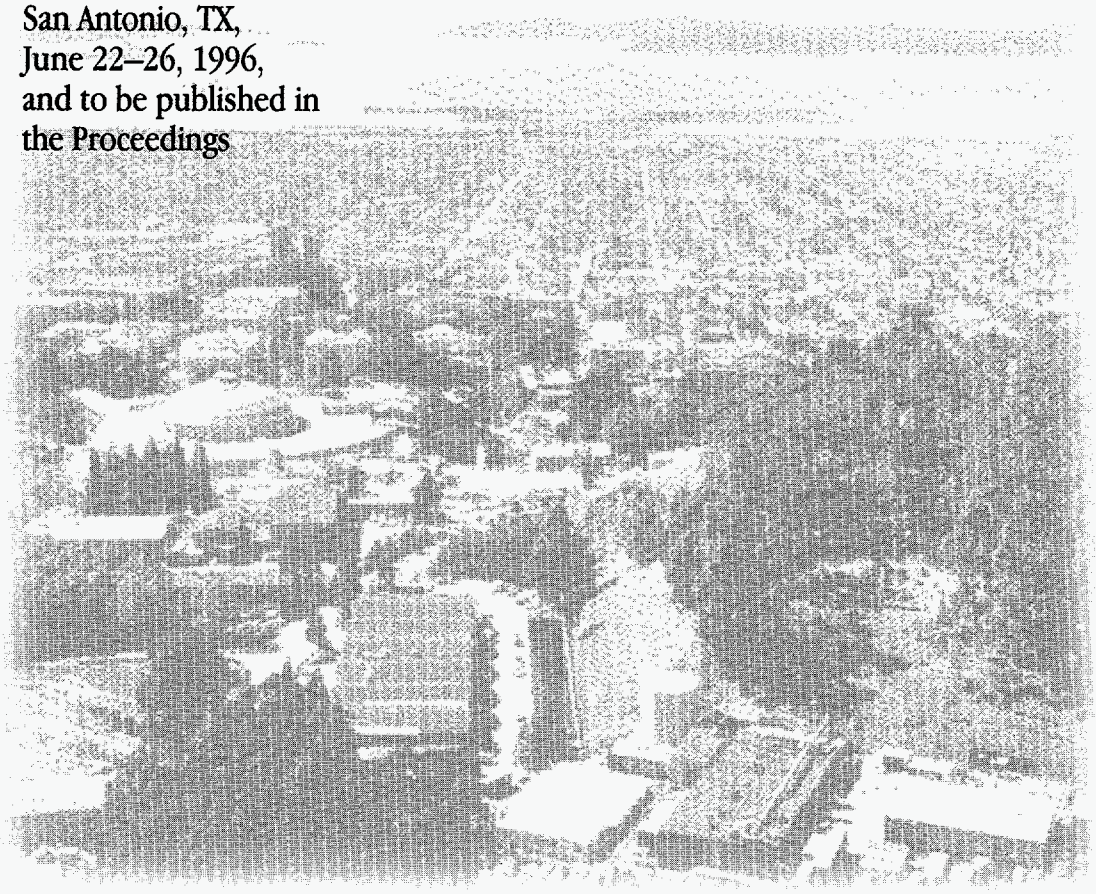

LBL-38117
TA-352

ASHRAE Transactions 1996, V. 102 PT. 2.

Surface Temperatures of Insulated Glazing Units: Infrared Thermography Laboratory Measurements

Brent T. Griffith, Daniel Türler, and Dariush Arasteh
Building Technologies Program
Energy and Environment Division
Lawrence Berkeley National Laboratory
University of California
Berkeley, CA 94720 USA

December 1995

This work was supported by the Assistant Secretary for Energy Efficiency and Renewable Energy, Office of Building Technologies, Building Systems and Materials Division of the U.S. Department of Energy under Contract No. DE-AC03-76SF00098.

Surface Temperatures of Insulated Glazing Units: Infrared Thermography Laboratory Measurements

Brent T. Griffith, Daniel Türler, and Dariush Arasteh
Building Technologies Program
Energy and Environment Division
Lawrence Berkeley National Laboratory
University of California
Berkeley, CA 94720 USA

Abstract

Data are presented for the distribution of surface temperatures on the warm-side surface of seven different insulated glazing units. Surface temperatures are measured using infrared thermography and an external referencing technique. This technique allows detailed mapping of surface temperatures that is non-intrusive. The glazings were placed between warm and cold environmental chambers that were operated at conditions corresponding to standard design conditions for winter heating. The temperatures conditions are 21.1°C (70°F) and -17.8°C (0°F) on the warm and cold sides, respectively. Film coefficients varied somewhat with average conditions of about 7.6 W/m²·K (1.34 Btu/h·ft²·°F) for the warm-side and 28.9 W/m²·K (5.1 Btu/h·ft²·°F) for the cold-side. Surface temperature data are plotted for the vertical distribution along the centerline of the IG and for the horizontal distribution along the centerline. This paper is part of larger collaborative effort that studied the same set of glazings.

Introduction

The condensation resistance of insulating glazing (IG) units is strongly influenced by the warm-side surface temperatures present while heat is flowing through the IG. These temperatures are determined by the environmental conditions that the IG is subjected to, the overall design of the glazing system, and the complex thermal interaction between spacer materials and convecting gases within the edge region of the IG. Low conductance spacers provide warmer surface temperatures around the perimeter of the IG by reducing thermal bridging between the two outermost panes of glass. Convection occurring within the IG also affects surface temperatures, causing cooler temperatures at the lower portion of the window. This internal convective effect varies with the width of the gap between glazing layers and the temperature differences across the gap as well as the number of layers used in the design.

Computer models are useful for predicting the heat flow through windows and are considered necessary for efforts to rate and label windows because of the wide variety of window products and the costs involved in testing each product. Models that can accurately predict the condensation characteristics of an IG need to predict the distribution of surface temperatures rather than the overall heat flow which has been the focus of most prior models. Thus, condensation resistance models should take into account the combined effects of internal convection and edge conduction, as well as the overall design of the glazing. The development and validation of such computer models can benefit from detailed experimental data on the surface temperatures found on IGs under standard environmental conditions.

This paper presents data on the distribution of surface temperatures for a set of IGs that were subjected to winter heating conditions in a laboratory. The data were gathered using infrared thermography which is a non-destructive method of mapping surface temperatures by measuring the thermal radiation emanating from the object (Arasteh et al. 1992). The seven different specimens were mounted between warm and cold environmental chambers and measured under steady state conditions that closely approximate standard ASHRAE conditions for winter heating. This paper is closely associated with additional papers by other authors that have either measured or modeled the same set of IGs (Sullivan et. al.1996; de Abreu et al.1996; Elmahdy 1996; Zhao et al. 1996).

Apparatus and Procedures

Insulating Glazing Specimens

Seven different IG specimens were obtained from a manufacturer of a glazing component. Six of the specimens had commercial silicone foam spacers while one specimen had a common aluminum spacer. The reduced thermal bridging of the foam spacers allows better isolation of the effects of internal convection. All the IGs were air filled and fitted with breather tubes to avoid fluctuations in gas concentration and pressure. The IGs are all 508 mm (20 in.) by 406 mm (16 in.) in size with thickness varying from 12.2 mm (0.48 in.) to 33.4 mm (1.32 in.).

Table 1 lists the specimens by their designation used in this paper and describes the design of each glazing system, the overall thickness of the IGs, and the thickness of the foam used to mount the specimens between the environmental chambers. Specimens were mounted in extruded polystyrene foam mask walls that have a constant thickness and a close fit around the IG. The warm side surfaces of the IG and the foam are flush to each other; the cold side surface of the IG is recessed from the foam surface to make up for

TABLE 1 Test Specimen Descriptions and Mounting

IG designation	type of glazing	nominal gap thickness mm (inch)	spacer material	overall IG thickness mm (inch)	mask wall thickness mm (inch)
IGU#1A	Double, clear	12.5 (0.5)	foam	18.0 (0.71)	20.0 (0.79)
IGU#1B	Double, clear	12.5 (0.5)	foam	18.0 (0.71)	39.4 (1.55)
IGU#2	Double, clear	12.5 (0.5)	aluminum	18.5 (0.72)	20.0 (0.79)
IGU#3	Double, clear	6.4 (0.25)	foam	12.2 (0.48	20.0 (0.79)
IGU#4	Double, clear	19 (0.75)	foam	25.0 (0.98)	26.2 (1.03)
IGU#5	Double, low-e	12.5 (0.5)	foam	18.3 (0.72)	20.0 (0.79)
IGU#6	Triple, clear	12.5 (0.5) ea.	foam	33.4 (1.32)	39.4 (1.55)
IGU#7	Triple, clear	6.4 (0.25) ea.	foam	21.7 (0.86)	26.2 (1.03)

the smaller thickness of the IG compared to the foam. Three different thicknesses of foam mask walls were used to more closely achieve the desired flush mounting on the cold side as well as the warm side in order to have a more uniform flow of cold air. The IG/foam interface was sealed, on both sides, with vinyl tape that covered the glazing spacer region to the sightline. One of the IGs (IGU#1) was tested with two thicknesses of mask wall to help determine the effect of the mounting; this results in two data sets (IGU#1A and IGU#1B) for this glazing. Thin stripes of aluminum tape are adhered to the warm side of the foam mask wall along the horizontal and vertical centerlines of the IG; these are used to identify IG centerlines in the thermographic image.

Warm and Cold Environmental Chambers

Environmental chambers are used to generate steady-state heat flow across the test specimens. Figure 1 diagrams the chambers. The size of the opening between the warm and cold chambers is 1200 mm (48 in.) square.

The cold chamber is a commercial food freezer modified for parallel upward plenum airflow. Temperature is controlled using pulse-switched heaters in three zones. Control stability over time and variations across the width of the airflow are both within ± 0.1°C (0.2°F). Airflow plenum depth is adjusted to 100 mm (4 in.). A custom-built

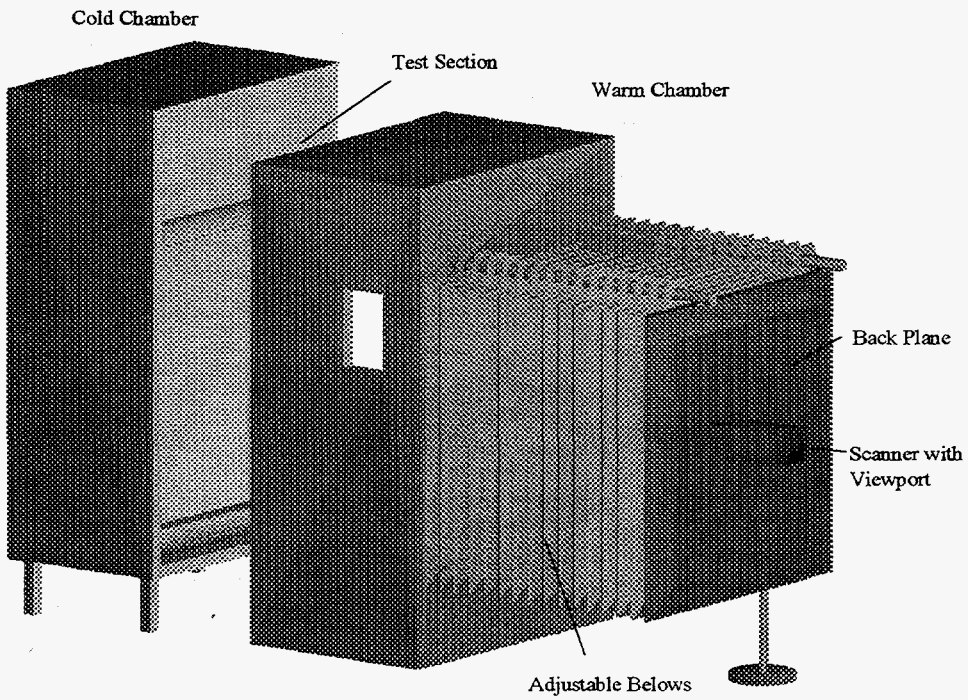

Figure 1 Infrared Thermography Laboratory Environmental Chambers

tangential blower drives air flow at velocities ranging from 3.9 to 5.2 m/s (8.7 to 11.6 mph) during the measurements reported here. Air velocity fluctuation at a given time is less than 0.2 m/s (0.4 mph). The variation in velocity from test to test is believed to arise from the gradual accumulation of ice in the air flow path.

The warm chamber is a special purpose apparatus developed for infrared thermography. Typical environmental chambers used for hot box type measurements use a plenum to direct warm air; however, this plenum would not allow viewing of the specimen. Therefore, the chamber has an unobstructed volume of air between the specimen and the IR scanner viewing port. An adjustable bellows allows locating the IR scanner from 1.5 m to 4.0 m (5 ft to 13 ft) away from the specimen. Air temperature is controlled in a recirculation zone within the subfloor. Air enters the subfloor at the base of the specimen and leaves at the rear of the subfloor. Air recirculates through a cooling coil and then across three zones of pulse-switched heaters. Variable fans allow airflow rates to change within the subfloor, so the air exchange rate the main chamber can change for some control of warm-side convective surface resistance.

Environmental Data Acquisition

The environmental chambers are controlled and monitored by a computer-based data acquisition system. The plug-in computer card has 16 channels with 12 bit analog to digital conversion, and is managed by its own operating system running on a 80486 processor. The 16 channels are multiplexed to a total of 128 single-ended analog inputs. Digital output capabilities operate solid-state relays used to switch heaters for temperature control. The processing card allows data to be preprocessed and reduced before it is fed to the regular computer data bus. Special software allows real-time display of data in graphs and tables. During normal operation, 72 channels are read to measure air temperatures, air velocities, mask wall surface temperatures, specimen surface temperatures, enclosure surface temperatures, relative humidity, thermocouple junction box temperature, and ground. Temperature probes include linear thermistor networks and type-T thermocouples. Figure 2 shows the location of some of the important sensors. Thermocouple junction temperature is compensated for by using three thermistors to measure temperature inside the insulated, isothermal zone box constructed of 12 mm (0.5 in.) aluminum plate. Thermocouple readings are adjusted to compensate for deviations found in prior calibrations of the system .

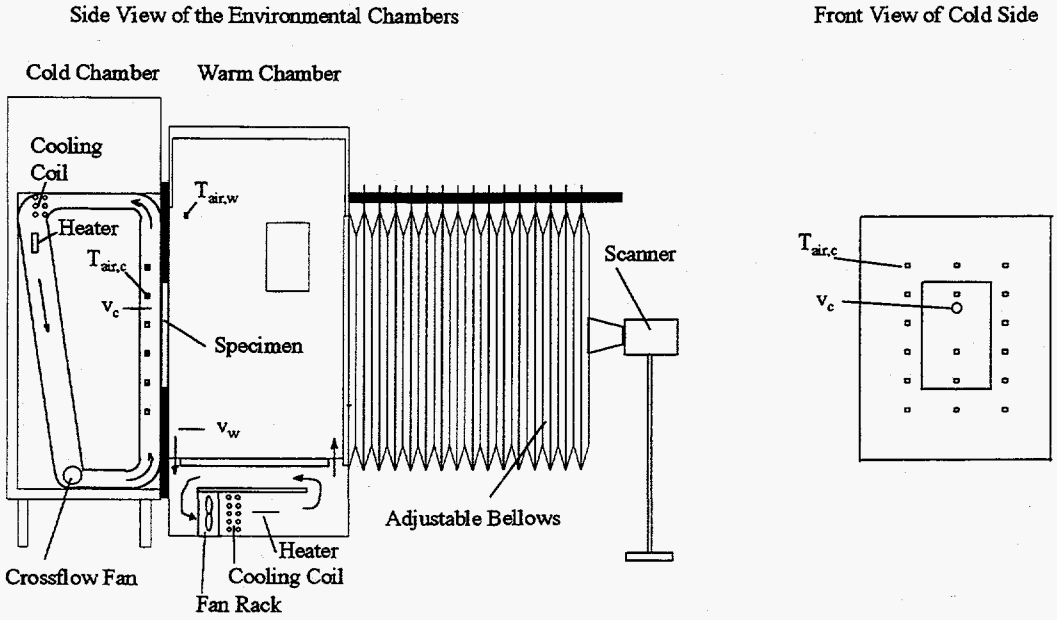

Figure 2 Schematic of Chambers with Sensor Locations

The data acquisition system collects 24 samples per second for each measurement which are averaged and then converted to engineering units. These averaged values are then passed to the PC every second and displayed in real time in order to monitor chamber performance. Data are stored in the computer for later postprocessing using a second averaging routine which takes the values averaged for each second and averages them again to yield one value per minute.

Thermistor measurements are used for temperature control in six separate zones, three in each chamber. These data are used to update individual proportional/integral/derivative (PID) controlling routines at a rate of six values per second. These routines output a series of pulse-width-modulation commands that control the on/off pattern of six heaters. Both chambers are cooled continuously and reheated in three zones to maintain the desired air temperature. The zones of conditioned air span across the width of the test section but are not physically separated. The controlling thermistor sensors are located in the air stream where the air begins to encounter the specimen.

A separate thermometer with two channels is used to continually verify the accuracy of air temperature measurements. This thermometer also measures the temperature of a custom infrared referencing target used in the thermographic measurements. This reference thermometer measures 100 Ω platinum resistance thermometer (PRT) probes using a 4-wire technique with a system accuracy of 0.01°C (0.02°F) (AC 1992). The system's calibration is traceable to the National Institute of Standards and Technology and uses the 1990 International Temperature Scale.

Infrared Thermography Equipment

A scanning-type, infrared (IR) imaging radiometer (scanner) was used to measure surface temperatures of the glazings. The IR scanner used here is a long-wave (8-12 μm), high-speed imager that uses a single detector (mercury/cadmium/telluride) to measure radiosity of the test specimen and reference targets (II 1989). The internal reference target located within the scanner head is complemented with two external reference targets located near the test specimen. These two external reference targets are separately controlled and measured for temperature. One is a commercial extended area blackbody with a well characterized emissivity that averages 0.97 and is controlled by thermoelectric elements (CIS 1992). The other reference target is a custom device with a glass surface and is controlled by circulating water through a copper plate. The IR scanner performs better as a relative temperature measurement device than as an absolute temperature measurement device. Therefore the addition of external referencing targets to the IR measurement system enables improvement in the absolute accuracy of the temperature measurements. The IR scanner data is fed into a computer which captures and averages frames of data in

order to gather data for postprocessing and to reduce noise in the measurements. The specified accuracy of the base IR scanner is ±2.0°C (3.6°F), however with external referencing and detailed procedures this accuracy is improved to ±0.5°C (0.9°F) (Griffith 1995). This reference contains a more detailed discussion of thermography and issues associated with its accuracy.

Infrared Thermography Procedures and Data Processing

This section describes the procedures used to gather the IR data presented in this paper. IR measurements are conducted at a minimum of four hours after the chambers have reached steady conditions. Humidity on the warm side is reduced so that specimens can be measured without condensation. The side-to-side thermal pattern on the specimen is monitored with the IR scanner prior to actual measurements to assure uniform conditions are present. The imaging distance was 1.5 m (3.2 ft.) which allows viewing the external reference targets and just over half the width of the specimen. The two external targets are located just left of the specimen at about the middle of the height. The image is focused on the specimen rather than the reference emitters which are closer by about 400 mm (16 in.). Emissivity is set at 0.86 for glass. This value for the emissivity of glass differs from the usual 0.84 and is generated by analyzing spectral data for glass and the response of the detector over only the 8-12 μm wavelengths; this value is also confirmed by measuring glass radiosity relative to known surfaces (e = 0.90) held at the same temperature. The background radiation level is quantified with an equivalent temperature by imaging a mirror before and after the measurements. This value is input into the thermography software to correct for emissivity and background reflections. The background level was between 20.6°C (69.1°F) and 21.5°C (70.7°F) for all the measurements. View angles are selected to avoid the scanner reflection. The environmental chambers are designed for a uniform background radiation scene.

The overall data for a tested specimen are gathered from two sets of measurements where each set is a close-up view. The first set of images is of the top and left quadrant of the IG specimen and the two external reference targets. The second set of images is of the bottom and left quadrant of the IG specimen and the two reference emitters. Sets of images are captured from each view with different scanner control settings for span and center temperature. Within a set of images there are geometry overlays that are captured uniformly with each image. The geometry overlays are narrow outlines oriented along the horizontal and vertical centerlines of the specimen and are used for later postprocessing of the temperature data. The span setting of the IR scanner determines the range, or bandwidth, of temperatures resolved by the scanner. The lowest span measurement (5°C) is the most accurate because the available resolution (8 bit) of the thermographic data is divided across the span being measured. Each set of images from a particular view

includes one 20°C (36°F) span image, one or two 10°C (18°F) span image(s), and two or more 5°C (9°F) span images where the number of multiple images depends on the range of temperatures present on the specimen. The multiple images of 5°C span data, with different center temperatures, allow covering the range of temperatures on the specimen with the better resolution measurements. In most instances the data reported are generated from compiled 5°C (9°F) span data, however the reference emitter has a minimum setpoint of 5.0°C (41°F) necessitating the use of 10°C (18°F) data when the coldest temperatures are much below 0°C (32°F).

Postprocessing of the temperature data involves extracting text data from the thermography software and then adjusting and combining data on a spreadsheet. The thermography software is used to process individual images in order to generate text data for the temperature profiles along the centerlines of the specimen. These temperature profiles extend halfway across the specimen for each image and are averaged over the width direction (about 25 mm [1 in.]) of the outline overlays in order to reduce noise in the data. The temperatures measured by the thermography system for the two reference targets are recorded and are used for scaling absolute temperature values. The final data are combined on a spreadsheet by first correcting the IR data for absolute value, then combining data from different images that have the same span but different ranges, and finally combining data from the top and the bottom close-up views. The geometric locations of the temperature data are determined by linearly distributing the data values across the overall length that the original outline overlay should correspond to on the actual specimen. The typical resolution in distance for the temperature data is less than 2 mm (0.08 in.) but the uncertainty in distance values is higher, about 3.7 mm (0.15 in.), because of the lower resolution of the actual IR scans, the readout resolution, and the aberrations resulting from viewing optics and perspective.

Test Conditions Analysis

This section presents the methods used to generate environmental data for each separate test. While the environmental chambers are controlled to provide nominally repeatable conditions and steady state heat transfer, the actual conditions for a particular test will vary from one test to another and will also deviate from the targeted standard design conditions. The environmental conditions are summarized in a concise way by reporting air temperatures and surface heat transfer coefficients, or film coefficients (see table 3 below). While film coefficients reported here are averaged values for the whole specimen surface, it is important to note that film coefficients actually have significant local variation. The radiative and convective components of the total film coefficient are reported for the warm side, while only the total is reported for the cold side.

The environmental data are deduced from the measurements recorded by the data acquisition system (described above) for air temperatures, specimen surface temperatures, mask wall surface temperatures, enclosure surface temperatures, and air speeds. These data are gathered in one minute bins of averaged values. These one minute values are then averaged over the time it takes to complete the thermographic measurements which typically requires 20 to 30 minutes. The warm side air temperature, $T_{air,w}$, is a spatial average of three thermocouples which are located about 120 mm (5 in.) off the mask wall and above the specimen. This is also the location of the controlling thermistors and is intended to measure the air supplied to the top of specimen before it is cooled by the specimen as it moves down. The cold side air temperature, $T_{air,c}$, is a spatial average of seventeen thermocouples which are located about 75 mm (3 in.) off the mask wall and throughout the middle of the test section.

Calibrated Transfer Standard Measurements

Prior experiments with the environmental chambers were conducted using a Calibrated Transfer Standard (CTS) (ASTM-1199 1990). These tests were run with the same chamber operation settings as were used for the IG measurements. The CTS measurements are used here to qualify a calculational model used to describe conditions during subsequent IG measurements. This film coefficient model combines an iterative analysis of the convection and a form factor analysis of the thermal radiation. The CTS measurements provide film coefficient data but it is difficult to apply these values directly to the IG tests because the overall heat flow is much lower (by a factor of 2 to 3) resulting in different surface temperatures and hence different air and radiation flows. Also the geometry of the CTS (900 mm (36 in.) square) does not match the IG specimens. Table 2 presents the results of measurements conducted with the CTS along with results of calculations using the warm-side film coefficient model described below.

TABLE 2 Comparison of Results from Warm-Side Film Coefficient Model and Measurements of Calibrated Transfer Standard (CTS)

Data set	**Warm-Side Measured**	**Warm-Side Modeled**				**Cold-Side Measured**
	$h_{tot,w}$ W/m²·K	$h_{tot,w}$ W/m²·K	$h_{conv,w}$ W/m²·K	$h_{rad,w}$ W/m²·K	$diff_{tot}$	$h_{tot,c}$ W/m²·K
1	8.42	8.02	3.25	4.77	-4.7%	35.1
2	8.11	7.76	3.28	4.48	-4.3%	30.1
3	8.06	7.78	3.28	4.50	-3.5%	29.8

Warm-Side Film Coefficient Model

A calculational model of the surface heat transfer coefficient was developed in order to provide film coefficient data for the warm side. Many alternative methods were evaluated to arrive at a model that had the most accuracy compared to the CTS data. The model has two parts, a convective part and a radiative part.

Convection. The convective part of the warm-side film coefficient is calculated using a literature correlation for natural convection with constant heat flux, equation (1) (Holman 1986). Figure 3 shows the heat flow situation and geometry. The analysis is oriented along the vertical center line of the specimen (x - axis in fig.3). The total height used in the analysis, **L**, is the sum of the height of the specimen, $\mathbf{H_{IG}}$, and the part of the mask wall above the specimen which is exposed to the warm side air flow. Equation (1) originates from an expression for the local film coefficient that has been integrated over the length, L.

$$h_{conv,w} = \frac{5}{4} k \; 0.60 \left(\frac{g \beta_w q_{conv,w}}{k_w \nu_{av}} \right)^{1/5} L^{4/5} \qquad (1)$$

The convective heat flux ,$\mathbf{q_{conv}}$, in equation (1) is also related to the convective coefficient, $\mathbf{h_{conv,w}}$, by the definition show in equation (2). The air temperatures, $\mathbf{T_{air,w}}$, and the mask wall temperatures, $\mathbf{T_{mw,w}}$, are measured by the data acquisition system; $\mathbf{T_{IG,w}}$ is measured by the thermography system and is an average of the IG surface data presented here (includes edge-of-glass). The mask wall above the specimen is included because the heat flow through it has an influence on the test conditions.

$$q_{conv,w} = h_{conv,w} (T_{air,w} - T_{surf,w}) \qquad (2)$$

$$\text{where, } T_{surf,w} = \frac{H_{IG} T_{IG,w} + T_{mw,w}(L - H_{IG})}{L}$$

Equations (1) and (2) form a system of equations and were solved by numerical iteration using a spreadsheet.

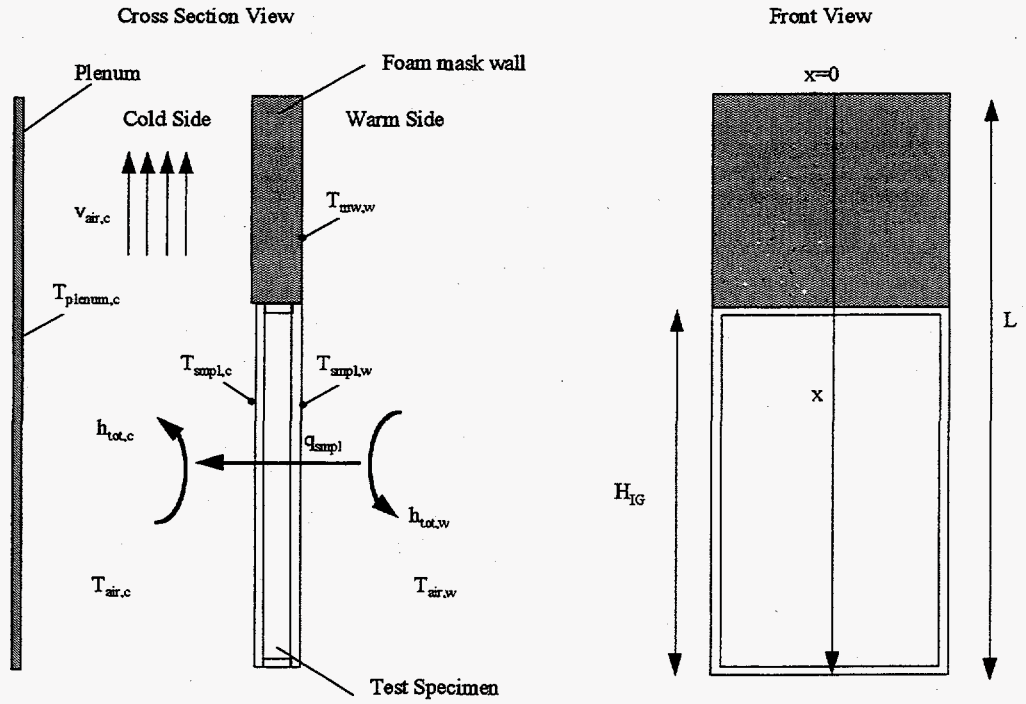

Figure 3 Geometry and Variables for Film Coefficent Analysis

Radiation. The radiative part of the warm side film coefficient is calculated using a detailed form factor analysis. The radiation surface coefficient will change because of variations in the surface temperatures of the enclosure surfaces as well as the specimen. The calculation is based on form factor analysis and assumes opaque, diffuse, gray-body surfaces. The IG specimens are specular, but since they are only slightly (16%) reflective, this complicating fact is ignored. A complete description of the specific radiative model is beyond the scope of this paper. Hence, only the basic equations are discussed in this paper.

The model of the warm chamber consists of 12 flat rectangular surfaces with area $\mathbf{A_n}$. Form factors, $\mathbf{F_{n-m}}$, determine the fraction of the total radiosity, $\mathbf{J_n}$, leaving surface n and arriving at surface m. For a complete enclosure the sum of all form factors associated with a single surface equals one. A total of 144 such form factors have been determined for the twelve surfaces of the warm chamber enclosure. The assumption of opaque surfaces neglects transmission effects, so the reflectivity, ρ, may be expressed as $\rho = 1 - \varepsilon$.

The net radiative heat flux, $q_{rad,n}$, for each surface, n, is described by equation (3). The incoming radiative heat flow, G_n, for each surface, n, is described by equation (4). The outgoing radiative heat flow, J_n, for each surface, n, is described by equation (5). Equations (3), (4), and (5) were solved simultaneously by numerical iteration using a spreadsheet.

$$q_{rad,n} = (G_n - J_n)/A_n \tag{3}$$

$$G_n = J_1 F_{1\text{-}n} + J_2 F_{2\text{-}n} + \ldots + J_{12} F_{12\text{-}n} \tag{4}$$

$$J_n = \varepsilon A_n \sigma T_n^4 + \rho G_n \tag{5}$$

The total radiative heat flux, $q_{rad,w}$, is calculated with equation (6). This equation takes the total radiation arriving at the colder specimen and subtracts the reflected and emitted portions.

$$q_{rad,w} = G_1 / A_{IG} - \rho_{IG} G_1 / A_{IG} - \varepsilon_{IG} \sigma T_{IG,w}^4 \tag{6}$$

The radiative part of the warm side film coefficient is then defined as shown in equation (7). This definition compares the heat flux to the temperature difference between the warm side air and the specimen surface.

$$h_{rad,w} = \frac{q_{rad,w}}{T_{air,w} - T_{IG,w}} \tag{7}$$

Equations (1) and (7) are combined to provide the overall film coefficient for the specimen surface on the warm side shown as equation (8).

$$h_{tot,w} = h_{conv,w} + h_{rad,w} \tag{8}$$

Cold-Side Film Coefficient

The model developed for the warm side is difficult to apply to the cold side because comparatively little surface temperature data are gathered for the cold side surfaces. For this reason it becomes necessary to use correlations for the cold-side coefficient that are derived from the CTS measurements. The cold side air velocity varies and this has a significant effect on the film coefficient which is dominated by the convective part. The cold-side film coefficient estimates shown in table 3 are derived from interpolating between CTS measurements based on the air velocities.

Results

Figures 4 through 10 show the results of surface temperature measurements for the eight sets of measurements of the seven different specimens. Each of these figures is plotted on the same scale for purposes of comparison. The upper plot is the vertical distribution of temperatures along the centerline of the IG. The lower plot is the horizontal distribution of temperatures along the centerline of the IG from the left edge to the middle of the IG. Interested readers may obtain computer files containing the data pairs directly from the authors (see http://eande.lbl.gov/BTP/WDG/IRlab/IRlab.html). The vertical data sets have about 270 pairs of data; the horizontal data sets have about 120 pairs of data. Uncertainty in the surface temperature is estimated at ±0.5°C (0.9°F). Uncertainty in the location data is estimated at ±3.7 mm (0.15 in.).

Table 3 shows the environmental conditions at the time of each of the eight tests. Uncertainty in the temperature measurements shown in Table 3 is estimated at ± 0.05°C (0.1°F). The cold-side film coefficients are estimated to be accurate to within about 11%. The warm-side film coefficients are estimated to be accurate to within about 7%.

The experimental data presented are most useful as part of a larger collaborative study of the IG specimens. The reader is thus encouraged to compare the results presented here with the results of others who have measured or modeled the same IGs.

Figure 4 shows the results from tests IGU#1A and IGU#1B which have different mask wall thicknesses. IGU#1B has the thicker mask wall which should result in reduced local film coefficients on the cold side at the edge due to the stepped change in surface geometry. The data show sill and jamb temperatures to be about 1.5 C (3F) warmer for this specimen at the coldest parts of these edge regions while there is little difference at the header edge region.

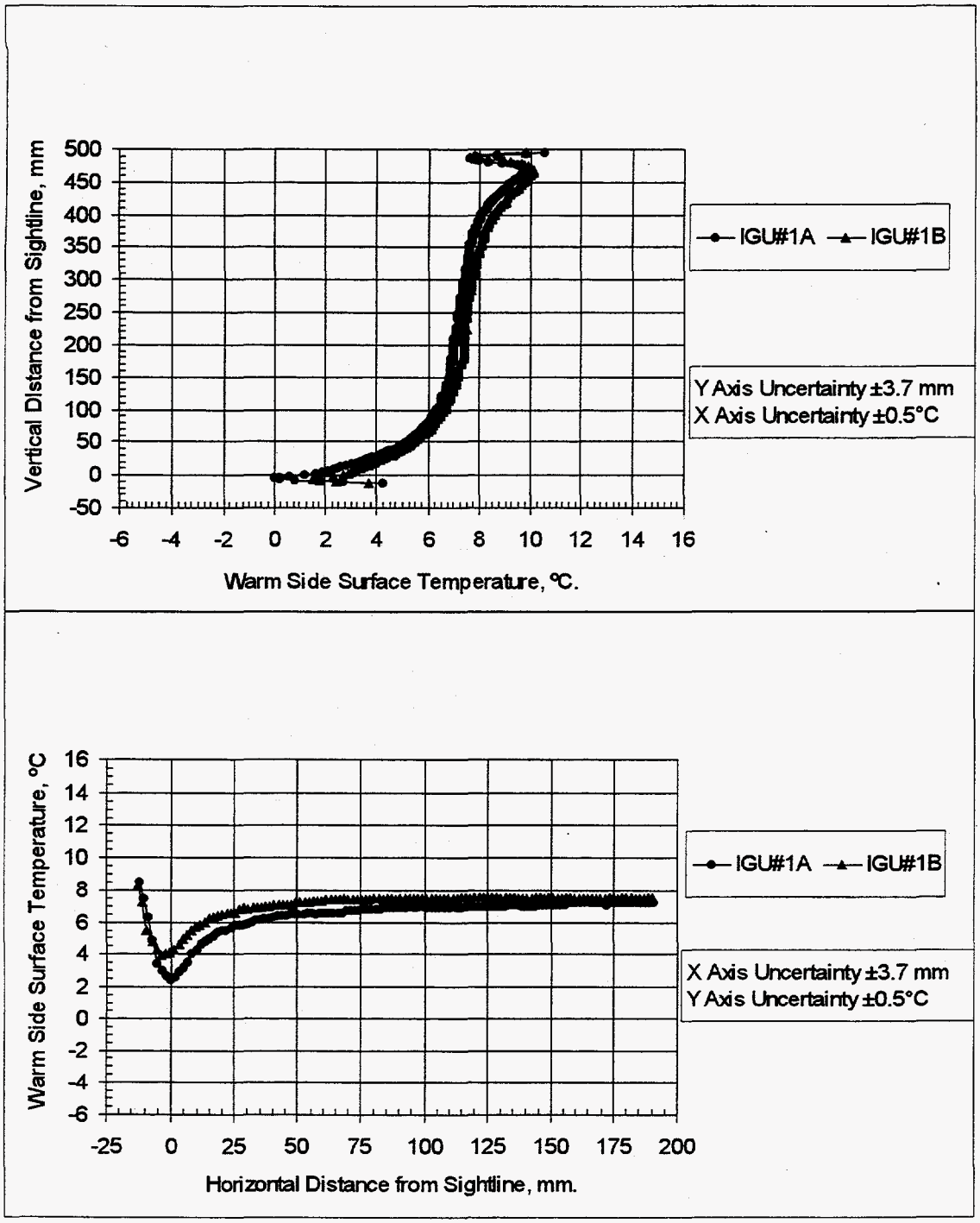

Figure 4 Temperature Distributions for IGU#1 tested with two different mask wall thicknesses

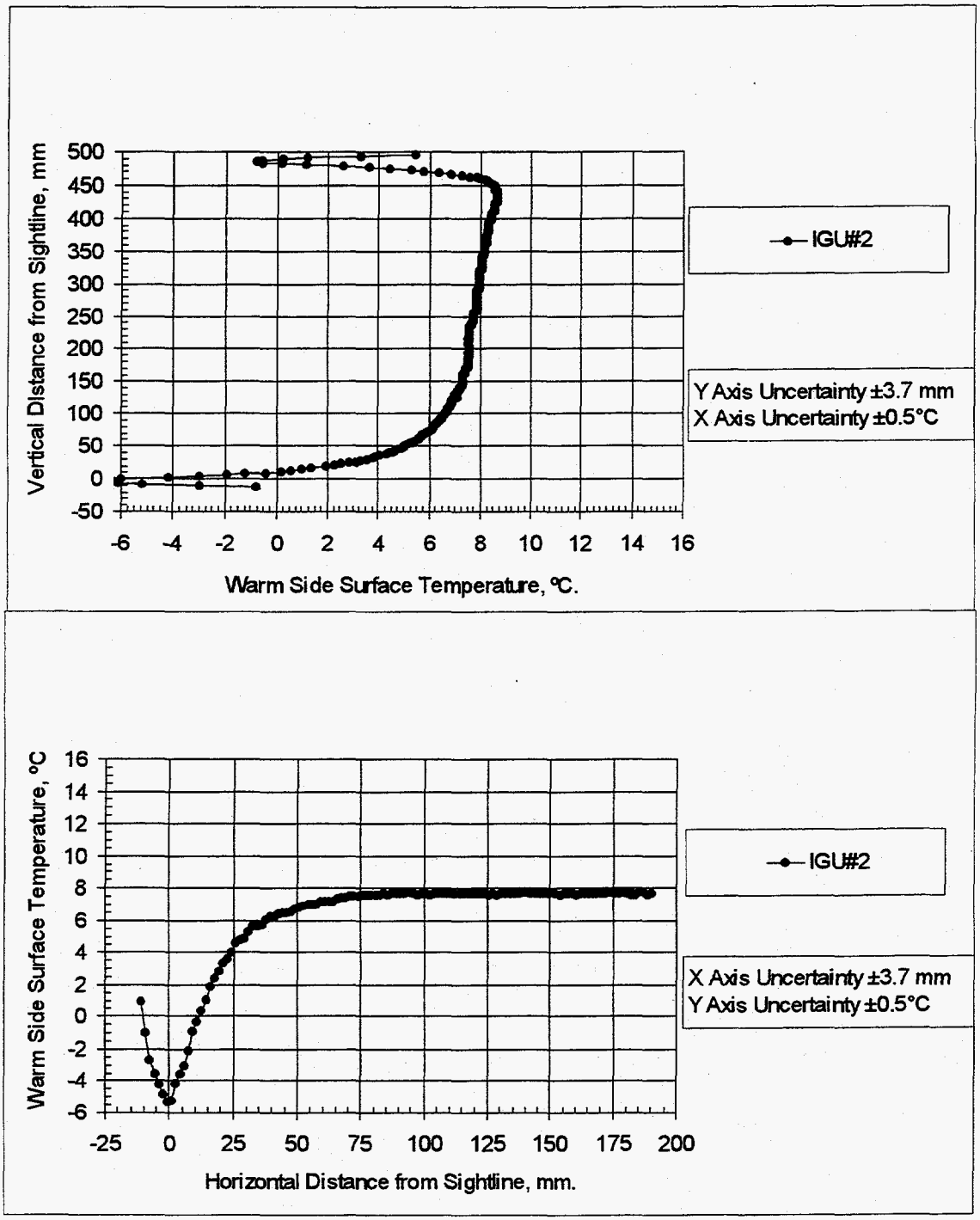

Figure 5 Temperature distributions for IGU#2

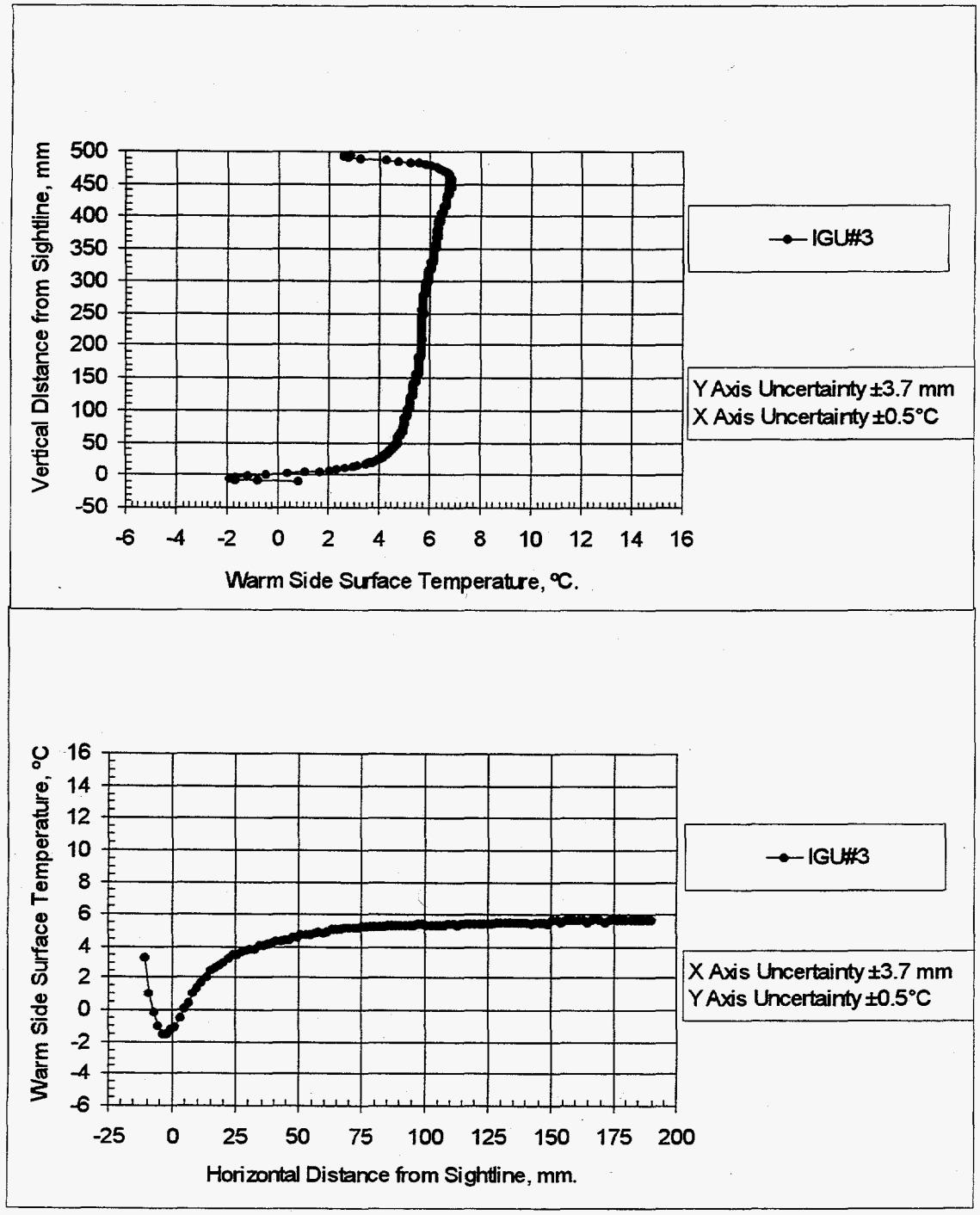

Figure 6 Temperature distributions for IGU#3

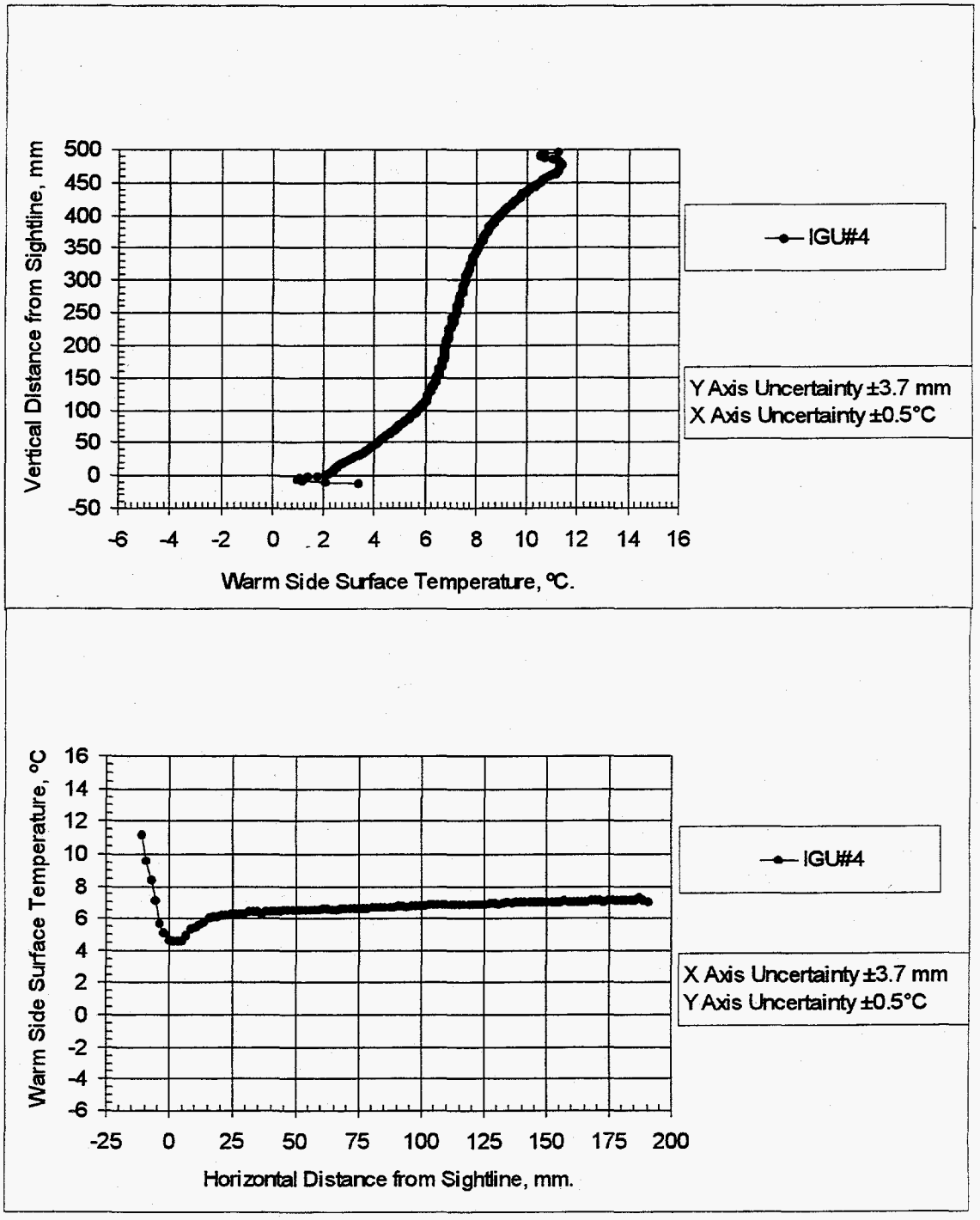

Figure 7 Temperature distributions for IGU#4

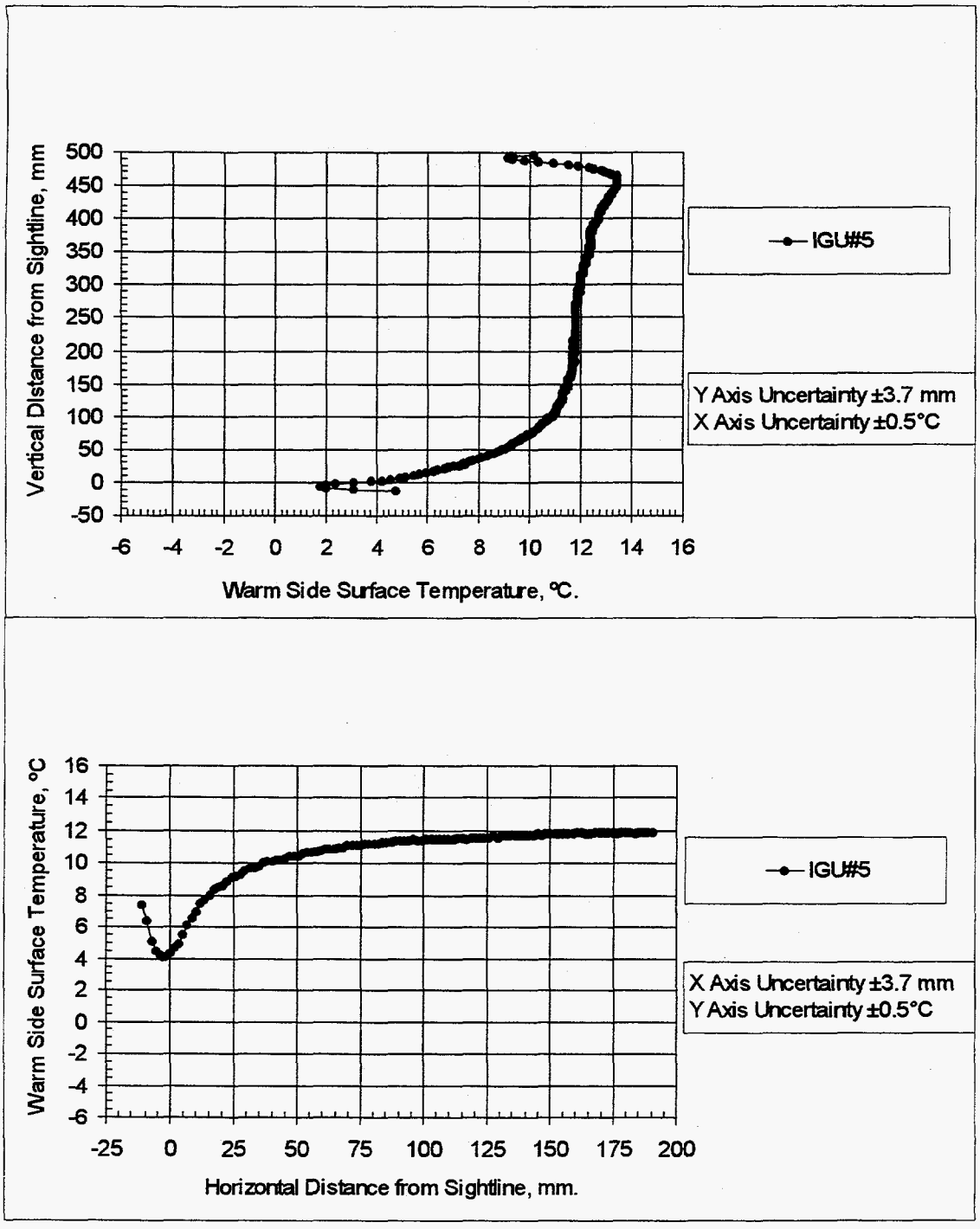

Figure 8 Temperature distributions for IGU#5

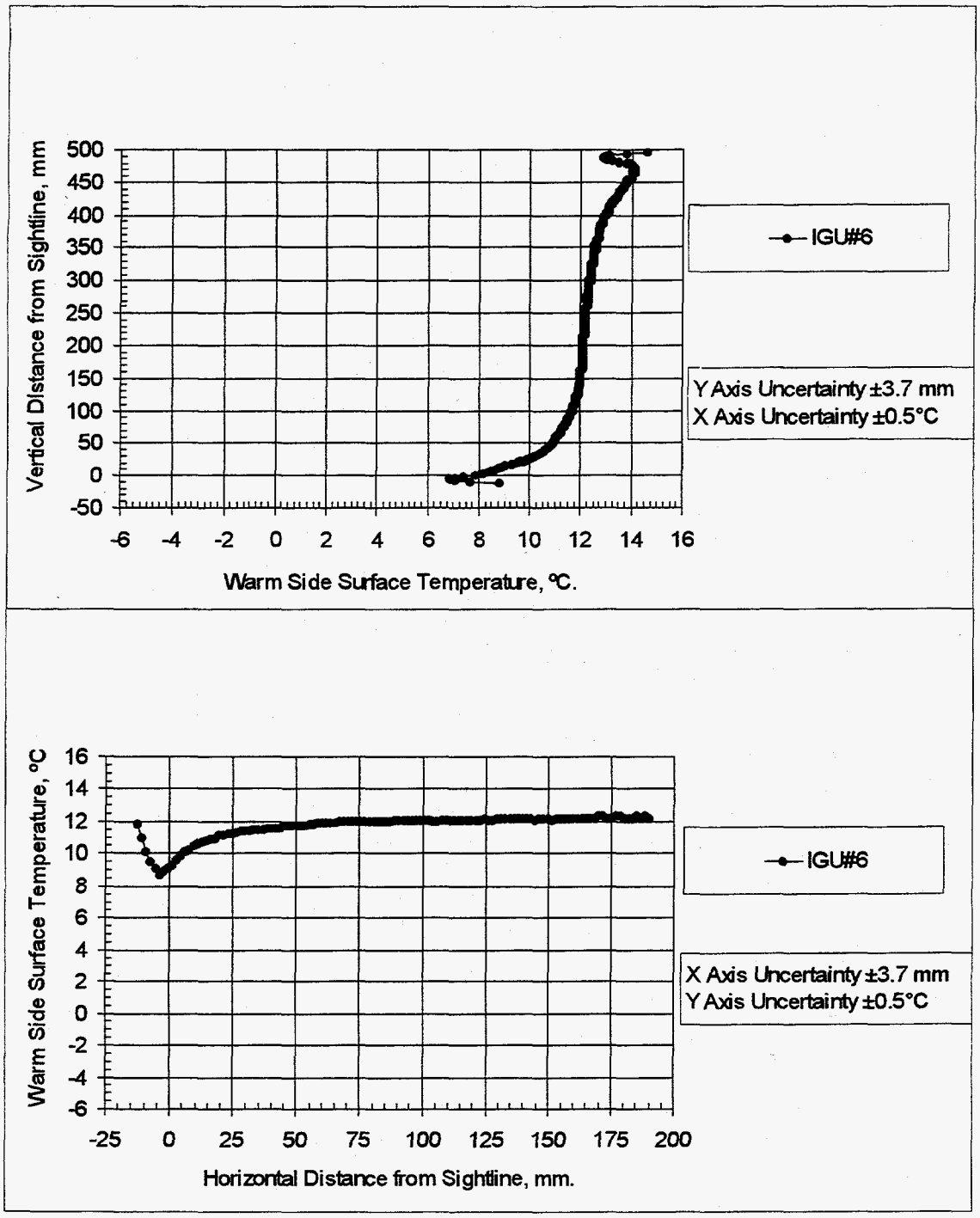

Figure 9 Temperature distributions for IGU#6

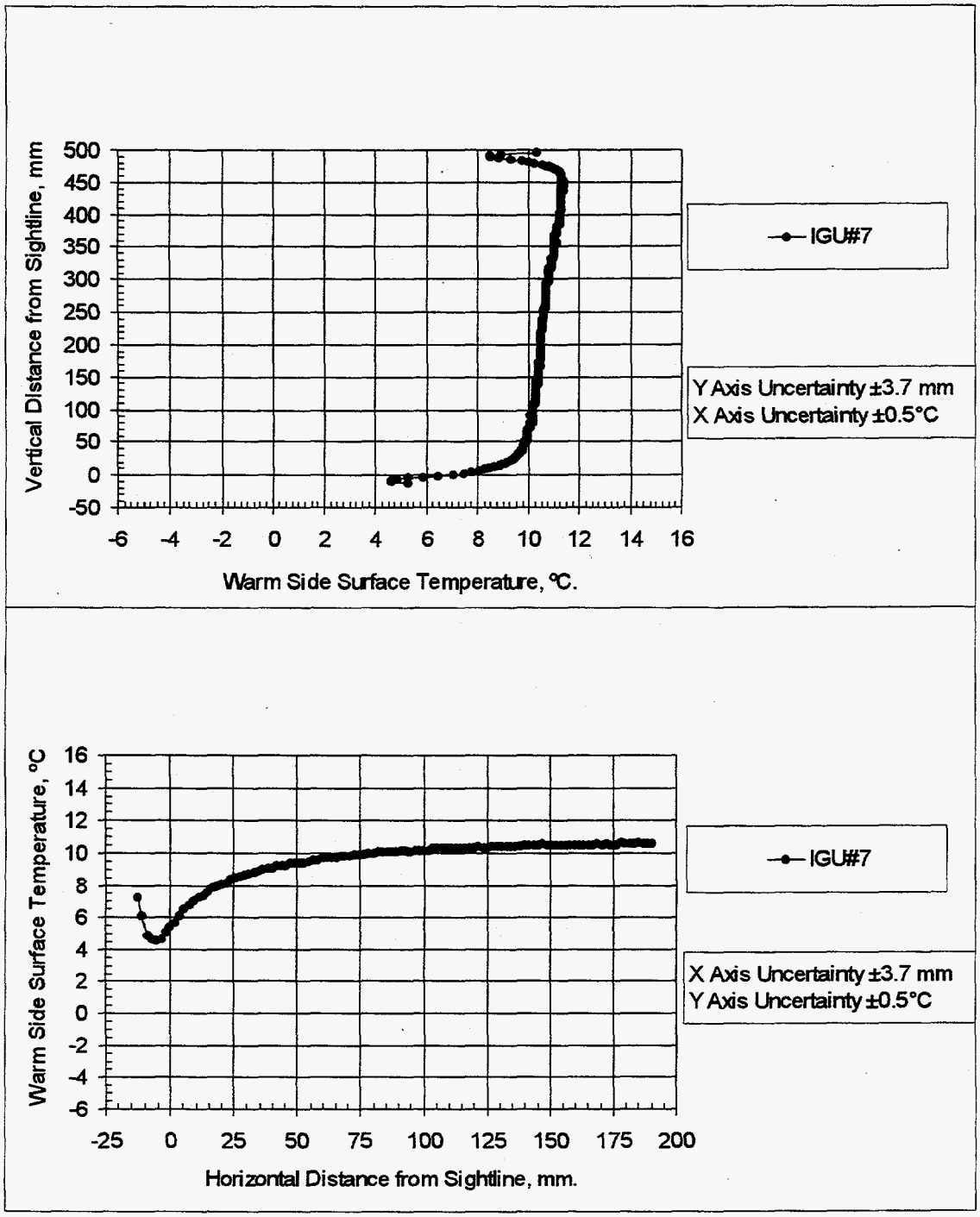

Figure 10 Temperature distributions for IGU#7

TABLE 3 Temperature Conditions and Film Coefficients for Specimen Measurements

	Warm-side				Cold-side	
	$T_{air,w}$ °C	$h_{tot,w}$ W/m²·K	$h_{conv,w}$ W/m²·K	$h_{rad,w}$ W/m²·K	$T_{air,c}$ °C	$h_{tot,c}$ W/m²·K
IGU#1A	21.12	7.65	3.19	4.46	-17.78	28.6
IGU#1B	21.11	7.58	3.07	4.51	-17.77	29.3
IGU#2	21.08	7.70	3.20	4.49	-17.78	29.0
IGU#3	21.12	7.69	3.26	4.43	-17.77	28.4
IGU#4	21.11	7.57	3.12	4.44	-17.78	30.8
IGU#5	21.23	7.72	2.97	4.76	-17.74	26.0
IGU#6	21.14	7.58	2.82	4.76	-17.77	29.5
IGU#7	21.10	7.47	2.94	4.48	-17.78	29.5

A number of interesting observations may be made by comparing the results for different glazings, however a thorough discussion is beyond the scope of this paper. Table 4 provides a summary of the results by listing various statistics of the temperature data sets gathered for each glazing. Averages are listed for the whole glazing (including the spacer region) and for the "center-of-glass" region based on the ASHRAE 63.5 mm (2.5 inch) definition for edge-of-glass. Gradient data are calculated for a 100 mm. (4 inch) distance about the center point of the glazing and are provided to give an indication of the strength of convection within the glazings. Note that this gradient is also driven by the localized nature of the warm side surface heat transfer coefficient.

Conclusions

Experimental data can be generated from infrared thermography that characterizes the distribution of surface temperatures on glazing systems under heat flow. This was done for a set of seven glazings and the data are useful for determining the condensation resistance of these glazing units as they were tested. The data are also useful for efforts to validate and develop computer simulation tools that model convection and edge conduction in glazing systems.

Table 4 Summary of Glazing Surface Temperature Measurement Results

IG designation	Average for Total glazing (°C)	Minimum (°C)	Maximum (°C)	Center point (°C)	Vertical Gradient for middle 100 mm DT/Dx (°C/m)	Average "center-of-glass" w/ standard edge defn. (°C)
IGU#1A	6.6	0.0	9.7	7.2	3.6	7.1
IGU#1B	7.1	1.5	10.1	7.5	3.0	7.5
IGU#2	6.1	-6.5	8.7	7.7	2.5	7.4
IGU#3	4.8	-1.9	6.9	5.7	2.0	5.6
IGU#4	6.8	1.0	11.4	7.2	7.2	7.0
IGU#5	10.6	1.8	13.4	11.8	2.0	11.6
IGU#6	11.8	6.9	14.1	12.2	2.0	12.2
IGU#7	9.7	4.7	10.7	10.6	2.5	10.4

The experimental measurements conducted here require careful procedures and detailed post processing of data in order to generate useful data. This makes it generally impractical to perform widespread measurements using these techniques for the direct testing of numerous different glazing products.

Acknowledgments

This work was supported by the Assistant Secretary for Energy Efficiency and Renewable Energy, Office of Building Technologies, Building Systems and Materials Division of the U.S. Department of Energy under Contract No. DE-AC03-76SF00098. The authors wish to thank Michael Glover and Dave Sergeant of Edgetech IG, Ltd. for providing the specimens used in the testing.

Nomenclature

A_n	= area of surface n (m^2)
CTS	= calibrated transfer standard
$diff_{tot}$	= difference between model and measured, %
e, ε	= emmissivity
F_{n-m}	= form factor between surfaces n and m
g	= gravitational constant (m/s^2)
G_n	= incoming radiosity (W)
$h_{conv,w}$	= warm-side convection coefficient ($W/m^2 \cdot K$)
$h_{rad,w}$	= warm-side radiation coefficient ($W/m^2 \cdot K$)
$h_{tot,c}$	= cold-side total film coefficient ($W/m^2 \cdot K$)
$h_{tot,w}$	= warm-side total film coefficient ($W/m^2 \cdot K$)
H_{IG}	= height of specimen (m)
IG	= insulating glazing
IGU#1	= IG specimen tested, designations 1 through 7
IR	= infrared
J_n	= outgoing radiosity (W)
k	= thermal conductivity of air ($W/m \cdot K$)
L	= overall length of convection (m)
PRT	= platinum resistance thermometer
$q_{conv,w}$	= heat flux due to convection, warm side (W/m^2)
$q_{rad,n}$	= heat flux due to radiation leaving surface n (W/m^2)
$q_{rad,w}$	= heat flux due to radiation, warm side (W/m^2)
$T_{air,c}$	= cold-side bulk air temperature (K)
$T_{air,w}$	= warm-side bulk air temperature (K)
$T_{IG,w}$	= warm-side average surface temperature of specimen (K)
$T_{mw,w}$	= warm-side surface temperature of mask wall (K)
T_n	= temperature of surface n (K)
$T_{surf,w}$	= warm-side surface temperature of specimen and mask wall (K)

Greek Symbols

β_w	volume coefficient of expansion (1/K)
ρ	reflectivity
Ω	ohm, nominal resistance
σ	Stefan-Boltsman constant ($W/m^2 \cdot K^4$)
ν_{av}	kinematic viscosity of air (m^2/s^2)

References

AC. 1992. Operation and maintence Instructions: A1011 Precision RTD Thermometer. Azonix Document F19-100257. Billerica, MA.: Azonix Corporation.

Arasteh, D.K., F. Beck, B.T. Griffith, N. Byars, and M. Acevedo-Ruiz. 1992. Using infrared thermography to study building heat transfer. *ASHRAE Journal* 34(10):34-38.

ASTM.1990b. ASTM C 1199, Standard test method for measuring the steady state thermal transmittance of fenestration systems using hot box methods. *Annual Book of ASTM Standards*, vol. 04.06: 671-682. Philadelphia, PA: American Society for Testing Materials.

CIS. 1992. SR 80 extended area infrared radiation source operation manual. Agoura Hills, CA.: CI Systems, Inc.

de Abreu, P., Fraser, R.A., Sullivan , H.F. and Wright, J.L., 1996. A study of insulated glazing unit surface temperature profiles using two-dimensional computer simulation. accepted for ASHRAE Transactions Vol. 102, Pt. 2.

Elmahdy, H. 1996 Surface temperature measurement of insulated glass units using infrared thermography. Accepted for ASHRAE Transactions Vol. 102, Pt. 2.

Griffith, B.T. F. Beck, D. Arasteh, and D. Turler. 1995. Issues associated with the use of infrared thermography for experimental testing of insulated systems. *Proceedings of the Thermal Performance of the Exterior Envelopes of Buildings VI Conference*. Atlanta, GA.:American Society of Heating, Refrigerating and Air-Conditioning Engineers.

Holman, J. P. 1986. *Heat transfer.* p 334 - 336. McGraw Hill.

II. 1989. Model 600L operator's manual. N. Billerica, MA.: Inframeterics, Inc.

Sullivan, H.F., Wright, J.L. and Fraser, R.A. 1996. Overview of a project to determine the surface temperatures of insulated glazing units: thermographic measurement and 2-D simulation. accepted for ASHRAE Transactions Vol. 102, Pt. 2.

Zhao, Y., D. Curcija, and W.P. Goss. 1996. Condensation resistance validation project - Detailed computer simulations using finite element methods. ASHRAE Transactions Vol. 102, Pt. 2.